Available online at www.sciencedirect.com
ScienceDirect
Trans. Nonferrous Met. Soc. China 24(2014) 1538−1546
Transactions of Nonferrous Metals Society of China
www.tnmsc.cn

Failure characteristics of three-body model composed of rock and coal with different strength and stiffness

Zeng-hui ZHAO[1,2], Wei-ming WANG[3], Chun-quan DAI[3], Ji-xing YAN[3]

1. State Key Laboratory of Mining Disaster Prevention and Control Co-founded by Shangdong Province and the Ministry of Science and Technology, Shandong University of Science and Technology, Qingdao 266590, China;
2. College of Mining and Safety Engineering, Shandong University of Science and Technology, Qingdao 266590, China;
3. College of Civil Engineering and Architecture, Shandong University of Science and Technology, Qingdao 266590, China

Received 17 May 2013; accepted 18 October 2013

Abstract: Four different types of three-body model composed of rock and coal with different strength and stiffness were established in order to study the failure characteristics of compound model such as roof−coal−floor. Through stress analysis of the element with variable strength and stiffness extracted from the strong−weak interface, the tri-axial compressive strength of the weak body and strong body near the interface as well as the areas away from the contact surface was found. Then, on the basis of three-dimensional fast Lagrangian method of continua and strain softening constitutive model composed of Coulomb−Mohr shear failure with tensile cut-off, stress and strain relationship of the four three-body combined models were analyzed under different confining pressures by numerical simulation. Finally, the different features of local shear zones and plastic failure areas of the four different models and their development trend with increasing confining pressure were discussed. The results show that additional stresses are derived due to the lateral deformation constraints near the strong−weak interface area, which results in the strength increasing in weak body and strength decreasing in strong body. The weakly consolidated soft rock and coal cementation exhibit significant strain softening behavior and bear compound tension−shear failure under uni-axial compression. With the increase of confining pressure, the tensile failure disappears from the model, and the failure type of composed model changes to local shear failure with different number of shearing bands and plastic failure zones. This work shows important guiding significance for the mechanism study of seismic, rock burst, and coal bump.

Key words: three-body model composed of rock and coal; strength near strong−weak interface; local shear band; plastic failure zone

1 Introduction

Western coal fields in our country are mainly located in the weakly cemented soft rock strata, such as mudstone, argillaceous sandstone, which show inferior stability with weak properties of poor weather resistance, easy to be softened in water, low intensity. Therefore, roadways have to be excavated in coal seam. However, many coal roadways are frequently associated with some mining disasters, such as roof burst, coal bump, and floor heave, which usually cause potential safety hazard for coal safety production. Actually, the mining area is a compound structure composed of roof, coal, and floor, and geological dynamics hazards in mining are clearly dominated by the general mechanical behavior of the whole model which is deeply related to the interaction between each unit [1−3]. Therefore, it has high actual application value to get deeper understanding of the interaction relationships between rock and coal with different mechanical properties and the damage evolution law of their composed model.

Many domestic and foreign scholars have focused their studies on the damage behavior of combined model of coal and rock. PETUKHOV and LINKOV [4] analyzed the stability of general bipartite system and roof-coal system while studying the stable behavior of rock mass after post-peak point. JIANG et al [5,6]

Foundation item: Project (51174128) supported by the National Natural Science Foundation of China; Project (20123718110007) supported by the Specialized Research Fund for the Doctoral Program of Higher Education of China
Corresponding author: Wei-ming WANG; Tel: +86-532-80681203; E-mail: tgzyzzh@163.com
DOI: 10.1016/S1003-6326(14)63223-4

studied the unstable sliding production condition of the combination of coal and rock samples by digital cameras and acoustic emission recorder which showed great significance for understanding the fault activation and coal bump. WANG et al [7] established an exact quantitative relation between dimension and compression strength as well as elastic modulus of coal rock by uni-axial compressive test. ZHANG et al [8] drew a conclusion that the damage development and increasing fracture in coal specimen could cause partial destruction in rock mass through the tri-axial compressive test of a assembly body composed of rock and coal. ZUO et al [9] and YANG et al [10] showed that the failure strength of two-body model under cyclic loading−unloading was higher than that under uniaxial loading. GUO et al [11] obtained the macro-failure mechanism of coal−rock combination bodies with different inclined angles by experimental and numerical simulation. ZHAO et al [12] achieved different kinds of forewarning messages before the failure of rock or coal samples through a thermal infrared system which showed that the stress of 90% of strength should be regarded as the stress-caution-point for the failure of bump prone coal. According to the acoustic−electromagnetic effect, DOU et al [13−15] found that the higher the strengths of coal seam and roof samples were，the stronger the rock burst liability, and the rock burst liability indexes increased with the height ratio of roof to coal. In addition, some numerical simulation results were put forward [16−18]. However, their findings are only applied to two-body model.

The above research results indicate that the global strength of composed model of coal-rock is better than that of the weak unit between coal and rock, and there exist large differences in mechanical behavior of combined model and single specimen. Mechanical properties of the single coal and rock specimen and their combination style have a great influence on the damage behavior of the composed model. However, all these observations are focused on the two-body model composed of coal and rock while some test results showed that the failure characteristics of three-body model composed of rock and coal were entirely different [19]. In view of this work, the aim is the three-body model. The results of laboratory tests show that property parameters of single coal and rock specimen have great dispersion. Besides, it is very difficult to get the soft rock samples from engineering site, so all of these make costly to launch an indoor test. On the contrary, it is flexible and efficient for the selection of model dimensions, material parameters and material constitutive model by numerical simulation method which posses a great advantage for engineering application.

In this work, four different types of three-body models composed of rock and coal with different strength and stiffness were established. Strength behavior near the strong−weak interface area of the model was discussed. Different features of local shear zone and plastic failure area of the four different models were simulated by employing the three-dimensional fast Lagrangian method of continua. All the results can provide theoretical reference for the mechanism study of the mining disasters.

2 Strength analysis of combined model

2.1 Four different types of combined model

Here, medium with high strength and stiffness is regarded as strong body, while the rest with poor property is considered weak body. Thus, there exist four combination styles for the three-body model composed of rock and coal as shown in Fig. 1. The four kinds of combination are strong−weak−strong (I type), weak−strong−weak (II type), weak−strong−strong (III type), strong−weak−weak (IV type).

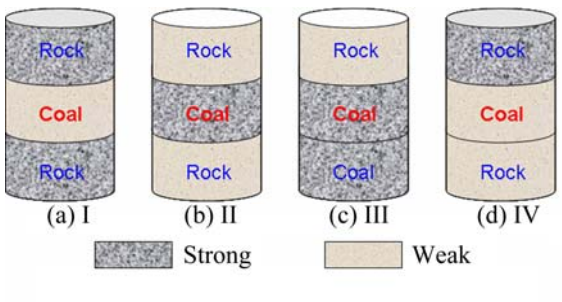

Fig. 1 Four combination styles of three-body model composed of rock and coal

2.2 Strength features of three-body model under tri-axial compressive stress

Let E_s, E_w, and μ_s, μ_w denote, respectively, the elastic modulus and Poisson ratio where the subscript s and w identify the strong and weak body, and suppose $E_s>E_w$, $\mu_s<\mu_w$, $\alpha=E_s/E_w$, $\beta=\mu_s/\mu_w$. In order to maintain the consistent lateral deformation at the strong−weak interface under compressive stress, the lateral deformation of weak body should be limited in a certain extent by strong body. Thus, the strong body exerts some restriction effect on the failure of weak body and restraint stress will be derived at the interface. Let $\sigma_1>\sigma_2\neq\sigma_3$, and assume that the compressive stress is positive. An element with variable parameters which contain strong and weak body is taken from the

neighborhood of interface shown in Fig. 2. Due to the mutual restriction between the two bodies, no shear stress exists on the contact surface. According to the superposition principle, total stresses on each element surface should include the original stress and restraint stress [20], namely,

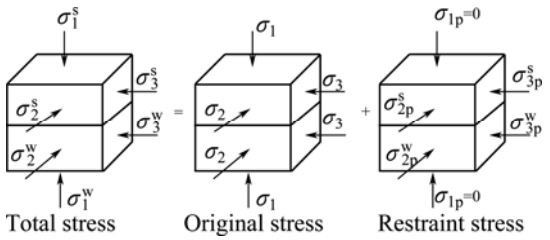

Fig. 2 Stress state of element with variable properties at strong−weak interface

$$\begin{cases}\sigma_1^{\mathrm{s}}=\sigma_1,\ \sigma_1^{\mathrm{w}}=\sigma_1\\ \sigma_2^{\mathrm{s}}=\sigma_2+\sigma_{2\mathrm{p}}^{\mathrm{s}},\ \sigma_2^{\mathrm{w}}=\sigma_2+\sigma_{2\mathrm{p}}^{\mathrm{w}}\\ \sigma_3^{\mathrm{s}}=\sigma_3+\sigma_{3\mathrm{p}}^{\mathrm{s}},\ \sigma_3^{\mathrm{w}}=\sigma_3+\sigma_{3\mathrm{p}}^{\mathrm{w}}\end{cases} \tag{1}$$

where subscript p denotes the restraint stress.

The restraint stresses are produced due to the difference of elastic modulus and Poisson ratio between strong and weak bodies. As shown in Fig. 3, the lateral deformation of strong body is smaller than that of weak body because of $E_{\mathrm{s}}>E_{\mathrm{w}}$, $\mu_{\mathrm{s}}<\mu_{\mathrm{w}}$. Hence, tensile stresses of $\sigma_{2\mathrm{p}1}^{\mathrm{s}}$ and $\sigma_{3\mathrm{p}1}^{\mathrm{s}}$ will be derived in strong body near the interface while compressive stresses of $\sigma_{2\mathrm{p}1}^{\mathrm{w}}$ and $\sigma_{3\mathrm{p}1}^{\mathrm{w}}$ occur in weak body in order to keep the lateral deformation in consistency. Similarly, other additional stresses appear in this area under the action of σ_2 and σ_3.

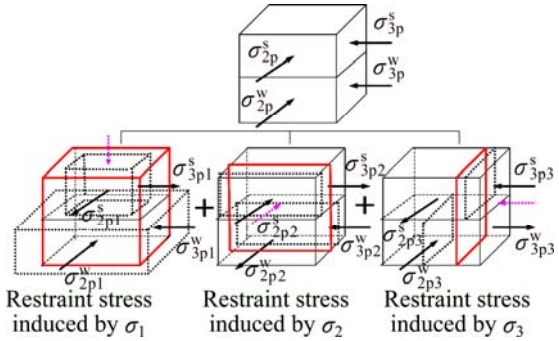

Fig. 3 Derived stresses on interface element

The total derived stresses on each element surface are calculated as follows using the superposition principle:

$$\begin{cases}\sigma_{2\mathrm{p}}^{\mathrm{s}}=-\sigma_{2\mathrm{p}1}^{\mathrm{s}}+\sigma_{2\mathrm{p}2}^{\mathrm{s}}-\sigma_{2\mathrm{p}3}^{\mathrm{s}}\\ \sigma_{3\mathrm{p}}^{\mathrm{s}}=-\sigma_{3\mathrm{p}1}^{\mathrm{s}}-\sigma_{3\mathrm{p}2}^{\mathrm{s}}+\sigma_{3\mathrm{p}3}^{\mathrm{s}}\\ \sigma_{2\mathrm{p}}^{\mathrm{w}}=\sigma_{2\mathrm{p}1}^{\mathrm{w}}-\sigma_{2\mathrm{p}2}^{\mathrm{w}}+\sigma_{2\mathrm{p}3}^{\mathrm{w}}\\ \sigma_{3\mathrm{p}}^{\mathrm{w}}=\sigma_{3\mathrm{p}1}^{\mathrm{w}}+\sigma_{3\mathrm{p}2}^{\mathrm{w}}-\sigma_{3\mathrm{p}3}^{\mathrm{w}}\end{cases} \tag{2}$$

According to the condition of static equilibrium, relationships between the derived stresses are

$$\begin{cases}\sigma_{2\mathrm{p}1}^{\mathrm{s}}=\sigma_{2\mathrm{p}1}^{\mathrm{w}},\ \sigma_{2\mathrm{p}2}^{\mathrm{s}}=\sigma_{2\mathrm{p}2}^{\mathrm{w}},\ \sigma_{2\mathrm{p}3}^{\mathrm{s}}=\sigma_{2\mathrm{p}3}^{\mathrm{w}}\\ \sigma_{3\mathrm{p}1}^{\mathrm{s}}=\sigma_{3\mathrm{p}1}^{\mathrm{w}},\ \sigma_{3\mathrm{p}2}^{\mathrm{s}}=\sigma_{3\mathrm{p}2}^{\mathrm{w}},\ \sigma_{3\mathrm{p}3}^{\mathrm{s}}=\sigma_{3\mathrm{p}3}^{\mathrm{w}}\end{cases} \tag{3}$$

The generalized Hooke laws for lateral strains are

$$\begin{cases}\varepsilon_2^{\mathrm{s}}=\dfrac{1}{E}[\sigma_2^{\mathrm{s}}-\mu(\sigma_1^{\mathrm{s}}+\sigma_3^{\mathrm{s}})]\\ \varepsilon_2^{\mathrm{w}}=\dfrac{1}{E}[\sigma_2^{\mathrm{w}}-\mu(\sigma_1^{\mathrm{w}}+\sigma_3^{\mathrm{w}})]\\ \varepsilon_3^{\mathrm{s}}=\dfrac{1}{E}[\sigma_3^{\mathrm{s}}-\mu(\sigma_1^{\mathrm{s}}+\sigma_2^{\mathrm{s}})]\\ \varepsilon_3^{\mathrm{w}}=\dfrac{1}{E}[\sigma_3^{\mathrm{w}}-\mu(\sigma_1^{\mathrm{w}}+\sigma_2^{\mathrm{w}})]\end{cases} \tag{4}$$

Deformation on the contact surface should satisfy the following relationship:

$$\varepsilon_2^{\mathrm{s}}=\varepsilon_2^{\mathrm{w}},\ \varepsilon_3^{\mathrm{s}}=\varepsilon_3^{\mathrm{w}} \tag{5}$$

Total stresses in the strong body near the interface are established as follows by combination of Eqs. (1)−(5):

$$\begin{cases}\sigma_1^{\mathrm{s}}=\sigma_1\\ \sigma_2^{\mathrm{s}}=\dfrac{-\lambda_1\sigma_1+\lambda_3\sigma_2-\lambda_2\sigma_3}{\lambda}\\ \sigma_3^{\mathrm{s}}=\dfrac{-\lambda_1\sigma_1-\lambda_2\sigma_2+\lambda_3\sigma_3}{\lambda}\end{cases} \tag{6}$$

Stresses in weak body near the interface are

$$\begin{cases}\sigma_1^{\mathrm{w}}=\sigma_1\\ \sigma_2^{\mathrm{w}}=\dfrac{\lambda_1\sigma_1+\lambda_3'\sigma_2+\lambda_2\sigma_3}{\lambda}\\ \sigma_3^{\mathrm{w}}=\dfrac{\lambda_1\sigma_1+\lambda_2\sigma_2+\lambda_3'\sigma_3}{\lambda}\end{cases} \tag{7}$$

where

$$\begin{cases}\lambda=(\alpha+1)^2-\mu_{\mathrm{w}}^2(\alpha+\beta)^2\\ \lambda_1=\mu_{\mathrm{w}}(\alpha-\beta)[\mu_{\mathrm{w}}(\alpha+\beta)+\alpha+1]\\ \lambda_2=2\alpha\mu_{\mathrm{w}}(1-\beta)\\ \lambda_3=2\alpha[\alpha+1-\mu_{\mathrm{w}}^2(\alpha+\beta)]\\ \lambda_3'=2[\alpha+1-\beta\mu_{\mathrm{w}}^2(\alpha+\beta)]\end{cases}$$

Strengths of the combined model far away the interface are confirmed by employing Coulomb−Mohr yield criterion:

$$\begin{cases}\sigma_{1\mathrm{s}}=\xi_{\mathrm{s}}\sigma_3+a_{\mathrm{s}}\\ \sigma_{1\mathrm{w}}=\xi_{\mathrm{w}}\sigma_3+a_{\mathrm{w}}\end{cases} \tag{8}$$

where $\xi_{\mathrm{s}}=(1+\sin\varphi_{\mathrm{s}})/(1-\sin\varphi_{\mathrm{s}})$, $\xi_{\mathrm{m}}=(1+\sin\varphi_{\mathrm{m}})/(1-\sin\varphi_{\mathrm{m}})$, $a_{\mathrm{s}}=2c_{\mathrm{s}}\cos\varphi_{\mathrm{s}}/(1-\sin\varphi_{\mathrm{s}})$, $a_{\mathrm{m}}=2c_{\mathrm{m}}\cos\varphi_{\mathrm{m}}/(1-\sin\varphi_{\mathrm{m}})$, φ_{s}, φ_{m} denote the friction angle, and c_{s}, c_{m} represent cohesion force, respectively.

The tri-axial compressive strength of strong body near the interface can be determined as follows by solving the resulting equations of Eqs. (6)−(8) simultaneously:

$$\sigma_{1c}^{s}=\frac{\xi_s(\lambda_3\sigma_3-\lambda_2\sigma_2)+\lambda a_s}{\lambda+\xi_s\lambda_1} \tag{9}$$

and the strength of weak body is

$$\sigma_{1c}^{w}=\frac{\xi_w(\lambda_2\sigma_2+\lambda_3'\sigma_3)+a_w\lambda}{\lambda-\xi_w\lambda_1} \tag{10}$$

Under the condition of axis symmetry compression, let $\sigma_2=\sigma_3$, and Eqs. (9) and (10) can be changed as

$$\begin{cases}\sigma_{1c}^{s}=\dfrac{\xi_s(\lambda_3-\lambda_2)\sigma_3+\lambda a_s}{\lambda+\xi_s\lambda_1}\\ \sigma_{1c}^{w}=\dfrac{\xi_w(\lambda_2+\lambda_3')\sigma_3+a_w\lambda}{\lambda-\xi_w\lambda_1}\end{cases} \tag{11}$$

Obviously, the differences of mechanical parameters between strong body and weak body will surely change the stress state of the area near contact interface. When $\alpha>1$, $\beta<1$, variations of the interface strength in two bodies compared with single specimen are

$$\begin{cases}\Delta\sigma_1^{w}=\sigma_{1c}^{w}-\sigma_{1w}>0\\ \Delta\sigma_{1c}^{s}=\sigma_{1c}^{s}-\sigma_{1s}<0\end{cases} \tag{12}$$

This implies that strength of the weak body is enhanced near the interface while strength of strong body is decreased, and the changed quantity of strength is directly related to elastic modulus and Poisson ratio. For the combination mode of strong−weak−strong (type I), strength of weak body will be significantly enhanced, and the smaller the thickness, the greater the amount of strength change, so this combination is beneficial to improve the global strength of the model. On the contrary, type II is the worst condition of combination which goes against the integral strength. If $\alpha=1$ and $\beta=1$, no derived stress will be produced at the interface, and strength of the combined structure depends on the weak medium.

3 Damage behavior analysis of combined model by numerical simulation

3.1 Calculation model

As shown in Fig. 1, let the diameter of combined model be 50 mm, and the ratio of height to diameter be 2, in which coal height is 30 mm, and heights of the upper and lower rock masses are 35 mm respectively. In order to meet the requirements of uniformity of the meshing, the model is divided into 48 units and 100 units in radial and height directions. Due to coal and rock masses from soft strata both showing softening behavior, a constitutive model composed of Coulomb−Mohr shear failure with tensile cut-off is adopted during the calculation. Strength parameters of friction angle and cohesion force are assumed to decay linearly with the equivalent plastic strain ε_{ps} during the post-peaking phase. According to displacement load method, loading rate is set as 1×10^{-8} m/s. The upper and lower ends are fixed where only the axial displacement is allowed. Pressure is applied to the circumferential outer surface to simulate the confining pressure. For the convenience of analysis, just one group of physical parameters for weak and strong body are given out based on laboratory test as shown in Table 1, and the data can be exchanged between rock mass and coal.

3.2 Calculation results

3.2.1 Comparison of stress−strain relations of different combinations

Figure 4 illustrates the stress−strain relations of different combinations when the confining pressure is set as 0, 2, 4, 6 MPa respectively.

The peak strengths of different combinations are all enhanced with the increase of confining pressures, because the fracture development and deformation during failure process in the weak part are limited by the confining effect which increases with the confining pressure. All stress−strain curves decrease rapidly after the peak point, and the model has a high stress drop which shows serious softening behavior. For the combination of type I, certain irreversible deformation occurs during the pre-peak stage which will consume energy, while no plastic strain appears in other model. Deformation modulus for each model in pre-peak phase is independent from the confining pressure, and each model almost has a same linear stage under different confining pressures respectively. However, the corresponding strain at peak point is magnified in each model with the increase of confining pressure, and the peak stress occurs in a larger plastic deformation. That is

Table 1 Mechanical parameters of specimens

Medium	Elastic modulus E/MPa	Poisson ratio μ	Initial cohesion force C_0/MPa	Initial friction angle φ_0/(°)	Residual cohesion force C_r/MPa	Residual friction angle φ_r/(°)	Threshold value of ε_{ps}/%	Tensile strength σ_t/MPa
Strong body	2100	0.252	3.5	44	0.7	38	0.4	1.11
Weak body	710	0.272	1.5	40	0.3	36	0.5	0.5

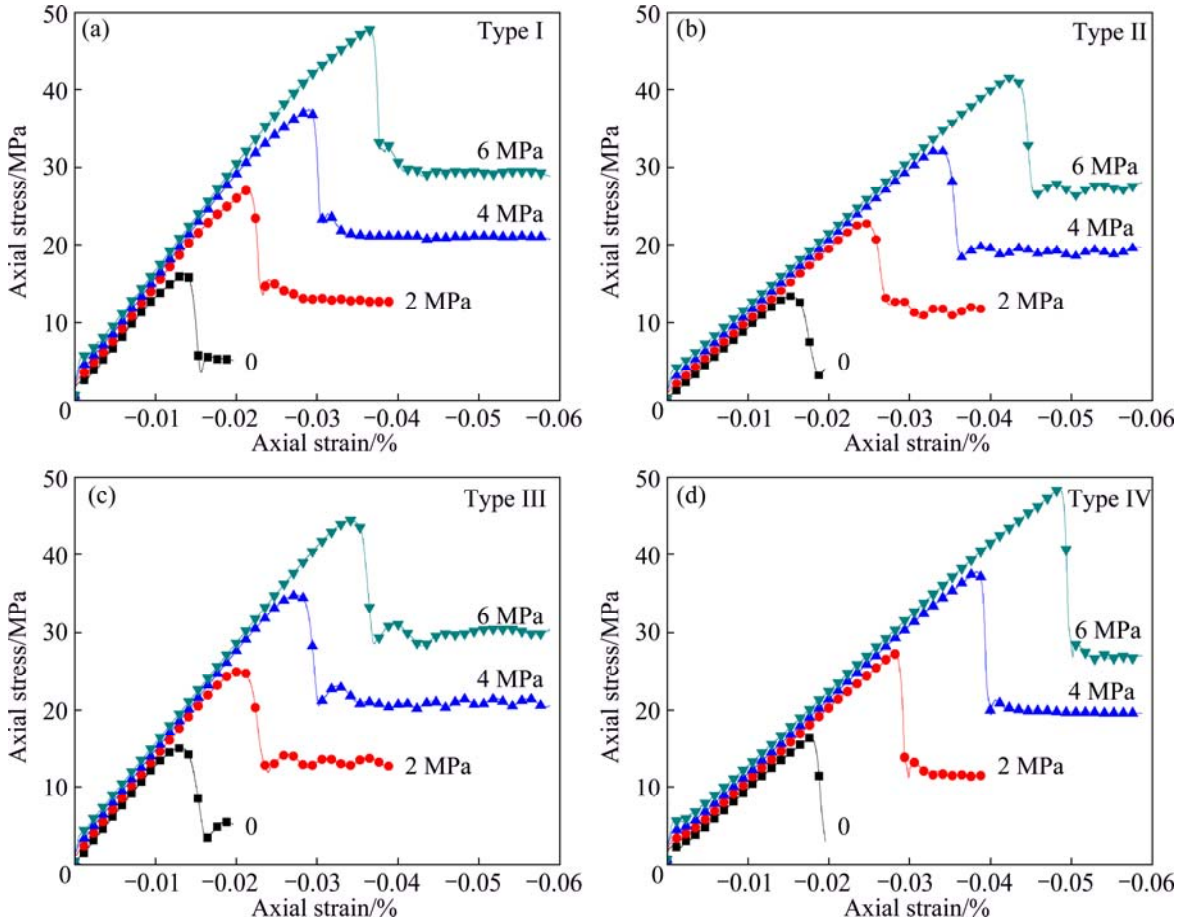

Fig. 4 Stress−strain relations of different combinations under different confining pressures

to say, the plastic performance of combined model is enhanced by increasing the confining pressure. In addition, the residual strength is also improved. There is almost no residual stage under uniaxial compression.

Figure 5 shows a comparison of the stress−strain features of the four different combinations under the action of a confining pressure 4 MPa. The result indicates that the order of peak strength is I>IV>III>II. It is evidence that combination of strong−weak−strong has the best strength while combination of weak−strong−strong bears the worst strength.

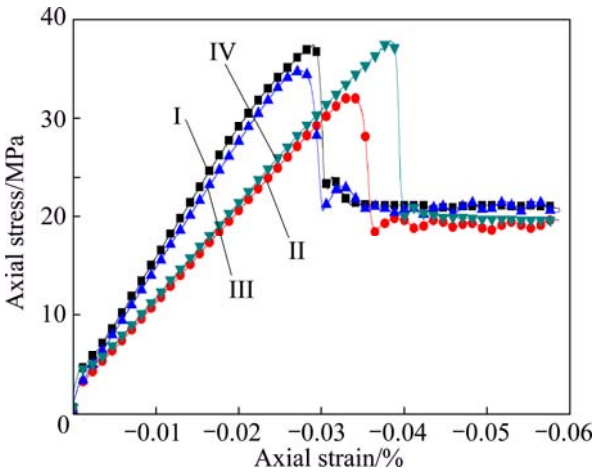

Fig. 5 Stress−strain relations of four assemblies under action of confining pressure 4 MPa

3.2.2 Analysis of localization failure in combined models

Due to the fact that the sampling interval is too small in Fig. 4, the strain softening of combined model shows the characteristic of stress drop after post peak. However, this is a misleading. The corresponding relation between strain softening stage in stress−strain curve and the unbalanced force under a confining pressure 2 MPa is magnified in Fig. 6, where the corresponding steps to peak stress and the maximum unbalanced force are brightly marked.

The progressive failures of combined model are often shown by some failure patterns. If the shear bands are concentrated in some certain region, the distribution of strain field becomes uneven and elements in this area are damaged seriously. The failure stages marked in the figure demonstrate the initiating and promoting stages of shear bands in different models. As a result of length reason, development process of the shear bands in each model is not presented, and only the final shapes are given out in Fig. 7. Distribution of the unbalanced force in some extent represents the damage condition of model elements, namely the dispersion and magnitude of

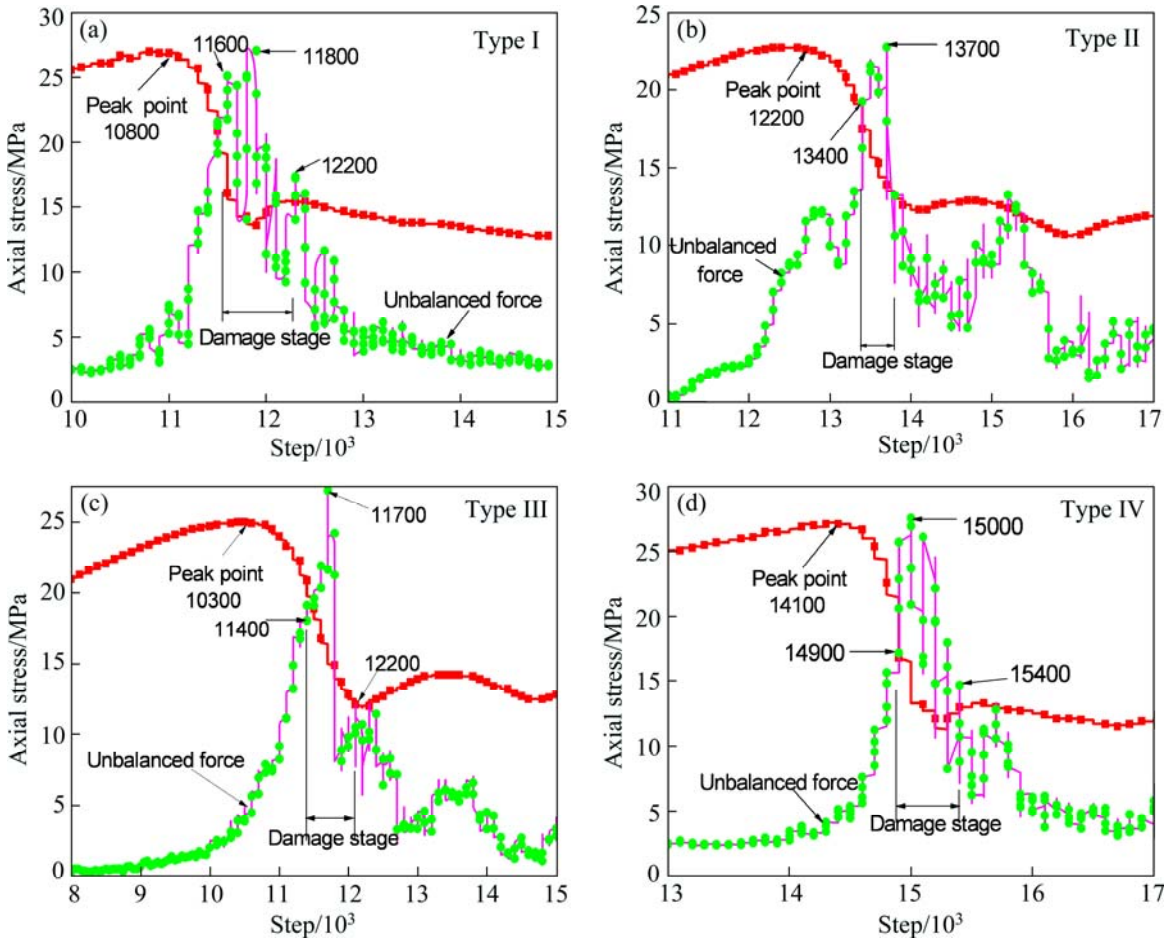

Fig. 6 Variation of stresses of four combinations with unbalanced force under confining pressure of 2 MPa

unbalanced force is on behalf of the damage dimensions. Development of shear bands is all launched in post-peak stage and formed in the initial period of residual stage.

Failure modes of the combined model are evidently affected by the confining pressure and the combination modes. The failure process and stage can be obtained by monitoring the shear strain increments in different load steps. Figure 7 shows the final localization shear bands in each model under different confining pressures. Three-dimensional shear zones and their distributions in the symmetry plane are both plotted. For the combination of type I, two conjugate shear zones are produced under uniaxial compression, and shear bands start from the central part of weak body (coal), and then gradually extend to the upper and lower rock mass. With the increase of confining pressure, shear deformation is concentrated in one of the main shear bands and the width is enlarged, meanwhile, another shear band is diminished in the weak body under the intersection point. Shear band networks appear in the middle part of combined model of type II when the confining pressure is 0. An obvious three-dimensional shear band is formed with the increase of confining pressure, and extends to the upper and lower weak bodies. However, the shear band does not extend to the upper and lower bounds due to the constrained effect at both ends. The length and inclined angle of shear bands in type II are significantly greater than those of type I. A shear band runs through the strong and weak body in type III under uniaxial compression, and the width is also enlarged with the increase of confining pressure. For type IV, the shear band is near horizontal in the middle weak body under uniaxial compression, and two shear bands appear in the middle and lower weak bodies with the increase of confining pressure.

Some conclusions are drawn from above analyses.

1) No matter what kind of combination modes, shear bands are all launched in the middle of weak body, and then extend to the strong body. In the post-peak stage, although the strength of weak body is lower than that of strong body, the strong body is also partially damaged due to the loading rate and the constraint effect at the interface.

2) Effects of confining pressure on the inclined angle of shear band are not obvious, but the width of shear band is enlarged with the increase of confining pressure.

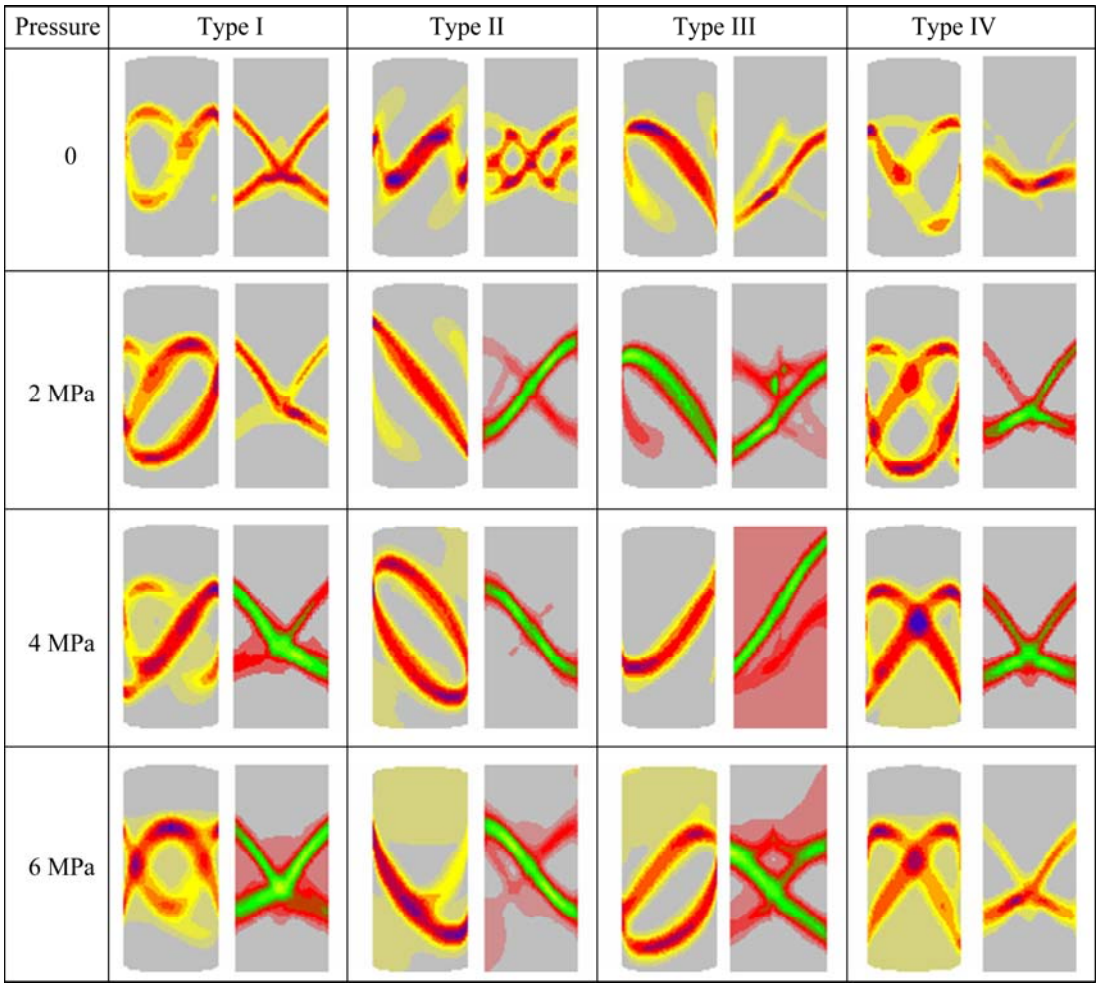

Fig. 7 Changes of shear bands of four models under different confining pressures

3) The number and distribution of shear bands are rather different in different combined models.

3.2.3 Distribution of plastic failure zones in different combined models

Figure 8 shows the distribution of plastic failure zones of the four different combined models under different confining pressures, where the distribution of shear failure areas is consistent with the shear bands in Fig. 5. When the confining pressure is increased to 6 MPa, the shear failure areas near the starting point of shear bands linked together, and the model bears global shear failure. In addition, widespread tensile failure zones occur near the interface area in type I, type III, and type IV under uni-axial compression. This is due to the changed stress state by the mutual interaction at the interface. With the increase of confining pressure, the tensile failure zone disappears, and the combined model presents global shear failure.

4 Conclusions

1) Due to the restraint of interface between strong and weak bodies, the total compressive strength and failure characteristics of three-body combined model are different from single specimen and two-body combined model. Strength of the weak body is enhanced near the interface while strength of strong body decreases, and the changed quantity of strength is directly related to elastic modulus and Poisson ratio of each medium. For the four different combined models, combination of strong−weak−strong has the best strength while combination of weak−strong−strong bears the worst strength.

2) The three-body model composed of soft rock and soft coal is produced evident shear bands under uni-axial compression and exhibits significant strain softening behavior under low confining pressure.

3) The width of shear band is enlarged with the increase of confining pressure which has no obvious effect on the inclined angle of shear band.

4) Under the condition of uni-axial compression, each combined model is subjected to the composite failure of shear and tension, but the tension failure zones disappear with the increase of confining pressure. Finally, the model only presents shear failure.

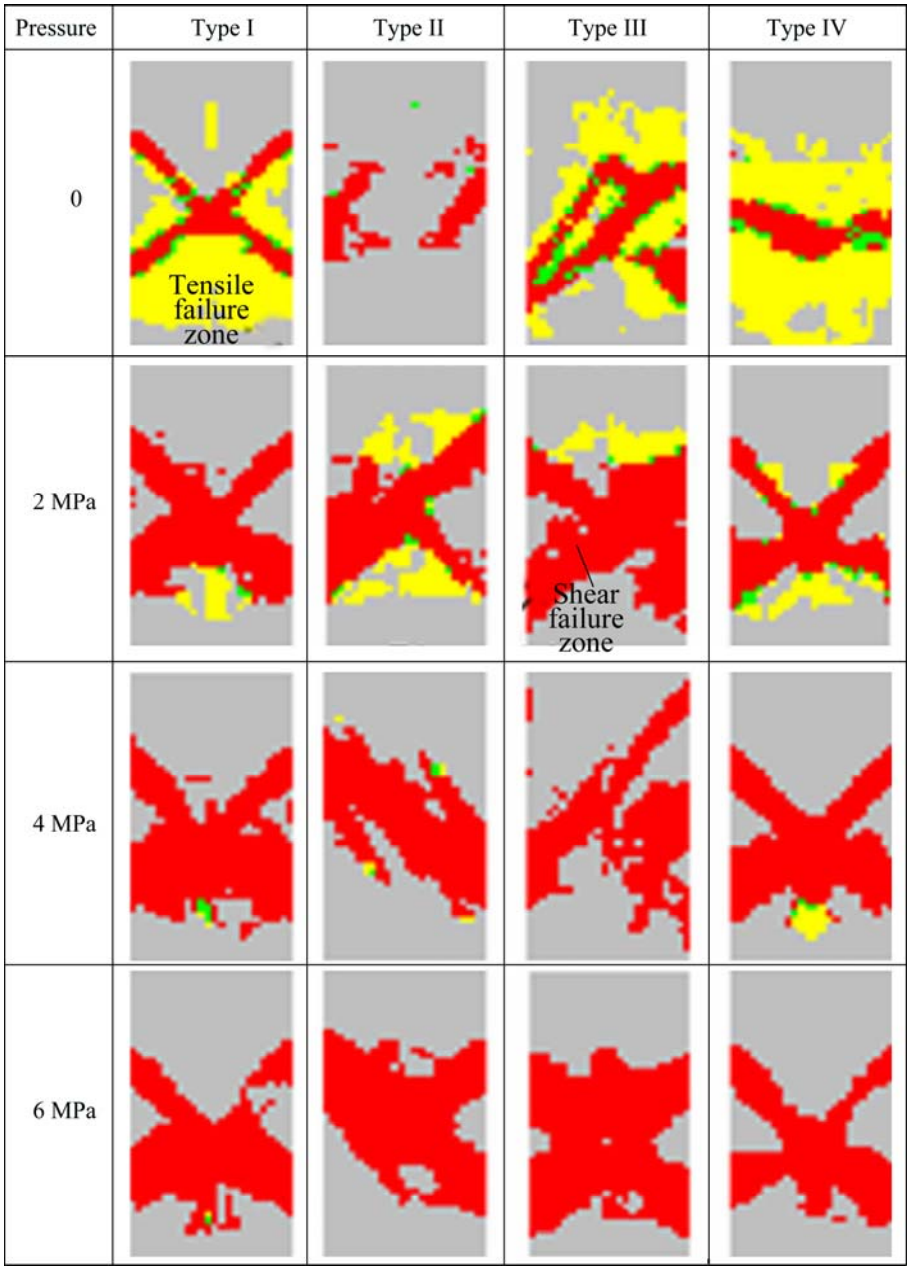

Fig. 8 Distribution of plastic failure zones of four models under different confining pressures

References

[1] XIE He-ping, CHEN Zhong-hui, ZHOU Hong-wei, YI Cheng, CHEN Zhi-jian. Study on two-body mechanical model based on interaction between structural body and geo-body [J]. Chinese Journal of Rock Mechanics and Engineering, 2005, 24(9): 1464−1487. (in Chinese)

[2] XIE He-ping, CHEN Zhong-hui, YI Cheng, ZHOU Hong-wei. Research on deformation and failure of interface based on interaction between structural body and geo-body [J]. Chinese Journal of Rock Mechanics and Engineering, 2008, 27(9): 1765−1780. (in Chinese)

[3] LIU Jian-xin, TANG Chun-an, ZHU Wan-cheng, YANG Tian-hong. Rock-coal model for studying the rockburst [J]. Chinese Journal of Geotechnical Engineering, 2004, 26(2): 276−280. (in Chinese)

[4] PETUKHOV I M, LINKOV A M. The theory of post-failure deformations and the problem of stability in rock mechanics [J]. International Journal of Rock Mechanics and Mining Sciences and Geomechanics Abstracts, 1979, 16(5): 57−76.

[5] JIANG Yao-dong, WANG Tao, SONG Yi-min, WANG Xin, ZHANG Wei. Experimental study on the stick-slip process of coal-rock composite samples [J]. Journal of China Coal Society, 2013, 38(2): 177−182. (in Chinese)

[6] JIANG Yao-dong, ZHAO Yi-xin, HE Man-chao, PENG Su-ping. Investigation on mechanism of coalmine bumps based on mesoscopic experiments [J]. Chinese Journal of Rock Mechanics and Engineering, 2007, 26(5): 901−907. (in Chinese)

[7] WANG Jian-bo, ZHU Zhen-de, LIU Jin-hui. Experimental and theoretical study on size effect of coal under uniaxial compression [J]. Water Resources and Power, 2013, 31(1): 50−52. (in Chinese)

[8] ZHANG Ze-tian, LIU Jian-feng, WANG Lu, YANG Hao-tian, ZUO Jian-ping. Effects of combination mode on mechanical properties and failure characteristics of the coal-rock combinations [J]. Journal of China Coal Society, 2012, 37(10): 1677−1681. (in Chinese)

[9] ZUO Jian-ping, XIE He-ping, MENG Bing-bing, LIU Jian-feng. Experimental research on loading-unloading behavior of coal-rock combination bodies at different stress levels [J]. Rock and Soil Mechanics, 2011, 32(5): 1287−1296. (in Chinese)

[10] YANG Yong-jie, SONG Yang, CHU Jun. Experimental study on characteristics of strength and deformation of coal under cyclic loading [J]. Chinese Journal of Rock Mechanics and Engineering, 2007, 26(1): 201−205. (in Chinese)

[11] GUO Dong-ming, ZUO Jian-ping, ZHANG Yi, YANG Ren-shu. Research on strength and failure mechanism of deep coal-rock combination bodies of different inclined angles [J]. Rock and Soil Mechanics, 2011, 32(5): 1333−1339. (in Chinese)

[12] ZHAO Yi-xin, JIANG Yao-dong, HAN Zhi-ru. Experimental study on acoustic and thermal infrared characteristics of bump-prone coal [J]. Chinese Journal of Rock Mechanics and Engineering, 2007, 26(5): 965−971. (in Chinese)

[13] DOU Lin-ming, TIAN Jing-cheng, LU Cai-ping, WU Xing-rong, MU Zong-long, ZHANG Xiao-tao, LI Zhi-hua. Research on electromagnetic radiation rules of composed coal-rock burst failure [J]. Chinese Journal of Rock Mechanics and Engineering, 2005, 24(19): 3541−3544. (in Chinese)

[14] LU Cai-ping, DOU Lin-ming, WU Xing-rong. Experimental research on rules of rockburst tendency evolution and acoustic-electromagnetic effects of compound coal-rock samples [J]. Chinese Journal of Rock Mechanics and Engineering, 2007, 26(12): 2549−2555. (in Chinese)

[15] CAO An-ye, DOU Lin-ming, LUO Xun. Seismic effort of blasting wave transmitted in coal-rock mass associated with mining operation [J]. Journal of Central South University, 2012, 19: 2604−2610.

[16] LI Xiao-lu, KANG Li-jun, LI Hong-yan, OUYANG Zhen-hua. Three-dimensional numerical simulation of bust-prone experiments about coal-rock combination [J]. Journal of China Coal Society, 2011, 36(12): 2064−2067. (in Chinese)

[17] WANG Xue-bin. Numerical simulation of deformation and failure for two bodies model composed of rock and coal [J]. Rock and Soil Mechanics, 2006, 27(7): 1066−1070. (in Chinese)

[18] FINZI Y, MUHLHAUS H, GROSS L, AMIRBEKYAN A. Shear band formation in numerical simulations applying a continuum damage rheology model [J]. Pure and Applied Geophysics, 2013, 170: 13−25.

[19] ZUO Jian-ping, XIE He-ping, WU Ai-ming, LIU Jian-feng. Investigation on failure characteristics and mechanical behavior of deep coal-rock single body and combined body under different confining pressures [J]. Chinese Journal of Rock Mechanics and Engineering, 2011, 30(1): 84−92. (in Chinese)

[20] TAN Xue-shu, XIAN Xue-fu. Theory and application of compound rock mass mechanics [M]. Beijing: China Coal Industry Publishing House, 1994. (in Chinese)

不同强弱组合下岩−煤−岩串联模型的破坏特征

赵增辉[1,2]，王渭明[3]，代春泉[3]，严纪兴[3]

1. 山东科技大学 矿山灾害预防控制省部共建国家重点实验室培育基地，青岛 266590；
2. 山东科技大学 矿业与安全工程学院，青岛 266590；
3. 山东科技大学 土木工程与建筑学院，青岛 266590

摘　要：针对不同强度煤、岩单元建立 4 种不同强弱组合的岩−煤−岩三元体串联模型。通过对强−弱交界面的应力状态分析，建立交界面附近区域强、弱体的三轴压缩强度；基于三维快速朗格朗日元法，强、弱体均采用 Coulomb−Mohr 剪切破坏和拉伸破坏的复合应变软化模型，数值模拟 4 种不同组合三元体模型在不同围压下的应力−应变曲线特征，分析不同组合的剪切破坏带及塑性破坏区随围压的变化趋势。结果表明：强−弱组合体交界面的层间约束作用会派生出附加应力，导致交界面附近区域强体强度变弱，弱体强度增强；弱胶结软岩体和煤体在单轴压缩下呈现拉剪破坏，表现出明显的应变软化行为，随着围压的增大，拉伸破坏消失，向整体剪切破坏发展，但不同组合下的破坏带数目及破坏区域不同。该研究对地震、岩爆、矿山冲击地压等灾害机理研究具有重要指导意义。

关键词：岩−煤−岩串联模型；强弱组合交界面强度；剪切带；塑性破坏区

(Edited by Xiang-qun LI)